Journal of Physics Communications

PAPER

Ion formation in an argon and argon-oxygen gas mixture of a magnetron sputtering discharge

R Hippler[1,2], M Cada[2], V Stranak[3] and Z Hubicka[2]

[1] Institut für Physik, Universität Greifswald, Felix-Hausdorff-Str. 6, D-17489 Greifswald, Germany
[2] Institute of Physics, Academy of Science of the Czech Republic, Na Slovance 2, 18221 Prague, Czech Republic
[3] University of South Bohemia, Faculty of Science, Branisovska 31, 37005 Ceske Budejovice, Czech Republic

E-mail: hippler@physik.uni-greifswald.de

Keywords: magnetron sputtering, ion mass spectrometry, molecular ion formation, negative ions

OPEN ACCESS

RECEIVED
21 February 2019

REVISED
23 April 2019

ACCEPTED FOR PUBLICATION
1 May 2019

PUBLISHED
20 May 2019

Abstract

Formation of singly and doubly charged Ar^{q+} and Ti^{q+} ($q = 1,2$) and of molecular Ar_2^+, $ArTi^+$, and Ti_2^+ ions in a direct current magnetron sputtering discharge with a Ti cathode and argon as working gas was investigated with the help of energy-resolved mass spectrometry. Measured ion energy distributions consist of low-energy and high-energy components resembling different formation processes. Intensities of Ar_2^+ and $ArTi^+$ dimer ions strongly increase with increasing gas pressure. Addition of oxygen gas leads to the formation of positively charged O^+, O_2^+, and TiO^+ and of negatively charged O^- and O_2^- ions.

1. Introduction

Plasma-based processing techniques are of considerable interest in fundamental research and industrial applications [1]. Plasma-assisted deposition of thin solid films is a major step in many applications, e.g. for magnetic recording media, electronic semiconductor devices, light emitting diodes, optical and hard coatings, solar cells, fuel cells, and batteries. Reactive plasmas with addition of a molecular gas are of particular importance in this context. For example, reactive magnetron sputtering in Ar/N_2 and Ar/O_2 gas mixtures and deposition of compound films was investigated by Affinito and Parsons [2]. A pronounced dependency of film properties on oxygen or nitrogen gas flow were observed. Deposition rate and film properties of nitride films (e.g. stoichiometry, electrical resistivity, index of refraction) as function of nitrogen gas flow in Ar/N_2 gas mixture was investigated by Mientus and Ellmer [3]. A theoretical model of reactive sputtering processes was developed by Berg and Nyberg [4]. Current voltage characteristics of magnetron discharges with oxygen were investigated by Depla *et al* and the observed behavior was linked to variations of the ion induced secondary electron emission [5]. Optical and mass spectrometric control of reactive plasmas was invented by Schiller *et al* [6] and Sproul and Tomashek [7, 8], respectively.

Film properties are frequently linked to particular properties of deposition plasma [9, 10]. In this context, the ion and energy influx into the growing film is of particular importance [11–18]. New and highly reactive species appear with the addition of oxygen to the discharge. Reactive oxygen species can have a large influence on the properties of deposited films [19]. In this paper we investigate the ion composition in a magnetron sputtering discharge with a titanium target. Recent measurements for pure argon gas are extended to larger gas pressures up to 5.5 Pa providing a clearer picture of the pressure dependency [20]. Positively and negatively charged ions are observed for an argon/oxygen gas mixture, resulting from gas phase collisions and from interaction with the sputtering target. Major differences are noticed to the pure argon case.

2. Experiment

The experimental set-up has been described in detail before [20–22]. The experiment is performed in a vacuum chamber which is pumped to a base pressure of less than 10^{-5} Pa. Argon (purity 99.999%) and oxygen gas

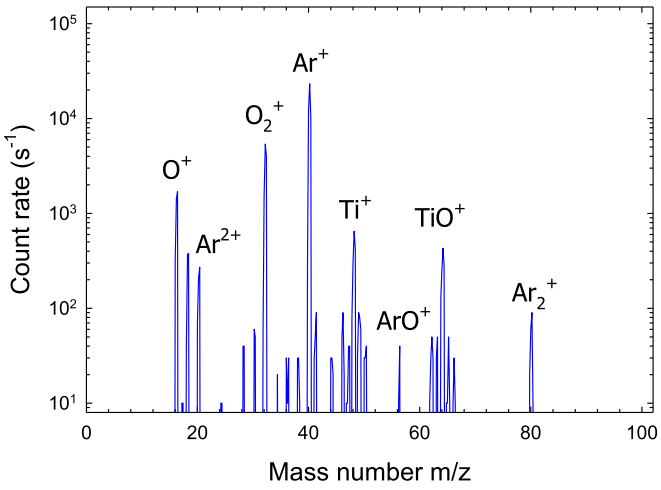

Figure 1. The mass spectrum of positive ions in the mass number range up to 100. Kinetic energy of detected ions $E = 0.25$ eV. $Ar + O_2$ gas mixture, gas flow rates 18 sccm + 6.4 sccm, respectively. Gas pressure 1.25 Pa. Discharge power $P = 150$ W.

(purity 99.995%) is admitted with the help of two gas flow controller. Argon and oxygen flow rates are set to 18 sccm and 6.4 sccm, respectively. With a ultrahigh vacuum gate valve between pump and chamber, the operating pressure is set in the range $p = 0.3$–5.5 Pa for pure argon and $p = 0.38$–3.8 Pa for the argon-oxygen gas mixture. A planar unbalanced magnetron is attached to the horizontal flange of the vacuum chamber which is equipped with a Ti target (diameter 50.8 mm, purity 99.7%). The magnetron plasma is ignited with the help of a DC power supply (Advanced Energy MDX–1 K) operated in the power regulation mode. Typical cathode voltages during operation at 150 W are 370 V and 250 V for argon gas pressures of 0.3 and 5.5 Pa, respectively, and 410 V and 350 V for $Ar+O_2$ gas pressures of 0.38 Pa and 3.8 Pa, respectively.

Energy-resolved mass spectrometry is performed with a commercial Hiden EQP 1000 mass/energy analyzer (Hiden Analytical Ltd., UK). Further details of the instrument and of the analyzer's settings can be found elsewhere [20]. The instrument is mounted opposite to the magnetron's race track at a distance of 45 mm from the cathode.

3. Results and discussion

A typical mass spectrum of positive ions in an $Ar+O_2$ gas mixture is shown in figure 1. The mass spectrum shows the main argon peak at $m/z = 40$ (relative abundance 99.6%), where m and z are the ion mass and ion charge number, respectively [23]. Titanium shows five stable isotopes in the mass range $m/z = 46$–50; the dominant mass peak at $m/z = 48$ has a relative abundance of 73.7% [23]. Doubly charged Ar^{2+} and Ti^{2+} ions are observed at $m/z = 20$ and 24, respectively. O^+ and O_2^+ ions are observed at mass numbers $m/z = 16$ and 32, respectively. ArO^+, TiO^+, and Ar_2^+ dimer ions appear at mass numbers $m/z = 56$, 64, and 80 (figure 1).

3.1. Ar

Energy distributions of singly charged Ar^+ and Ti^+ and doubly charged Ar^{2+} and Ti^{2+} ions are displayed in figure 2 for six different gas pressures ranging from 0.3 Pa to 5.5 Pa. The present measurements extend recent results for singly charged ions to larger pressures [20]. All energy distributions are plotted as a function of the scaled energy $\tilde{E} = E/q$, where E is the kinetic energy and q the charge number. The scaling allows for a presentation in a more compact form. The energy spectra of Ar^+ ions display a pronounced low-energy component with kinetic energies close to zero and a high-energy component which extends beyond 40eV. The two components show an opposite pressure dependency. The low-energy component strongly increases with increasing gas pressure while the high-energy component slowly disappears. The scaled energy distributions of all investigated ions appear rather similar, in particular, regarding the high-energy component. Energy distributions, hence, display a broad distribution or a maximum at the same scaled energy $\tilde{E} \approx 10$ eV. It indicates that the energy of doubly charged ions is about twice as large compared to singly charged ions. The present results are in agreement with a potential hump model of moving ionisation zones where ionisation occurs [24, 25]. The plasma density in these regions leads to a positive plasma potential (hump) that accelerates the newly born ions to kinetic energies proportional to the charge number.

Energy distributions of Ar_2^+ and $ArTi^+$ dimer ions are characterized by a pronounced low-energy peak resembling the fully thermalized ions from the plasma (figures 3(a) and (b)). At the lowest pressures of 0.3 Pa and

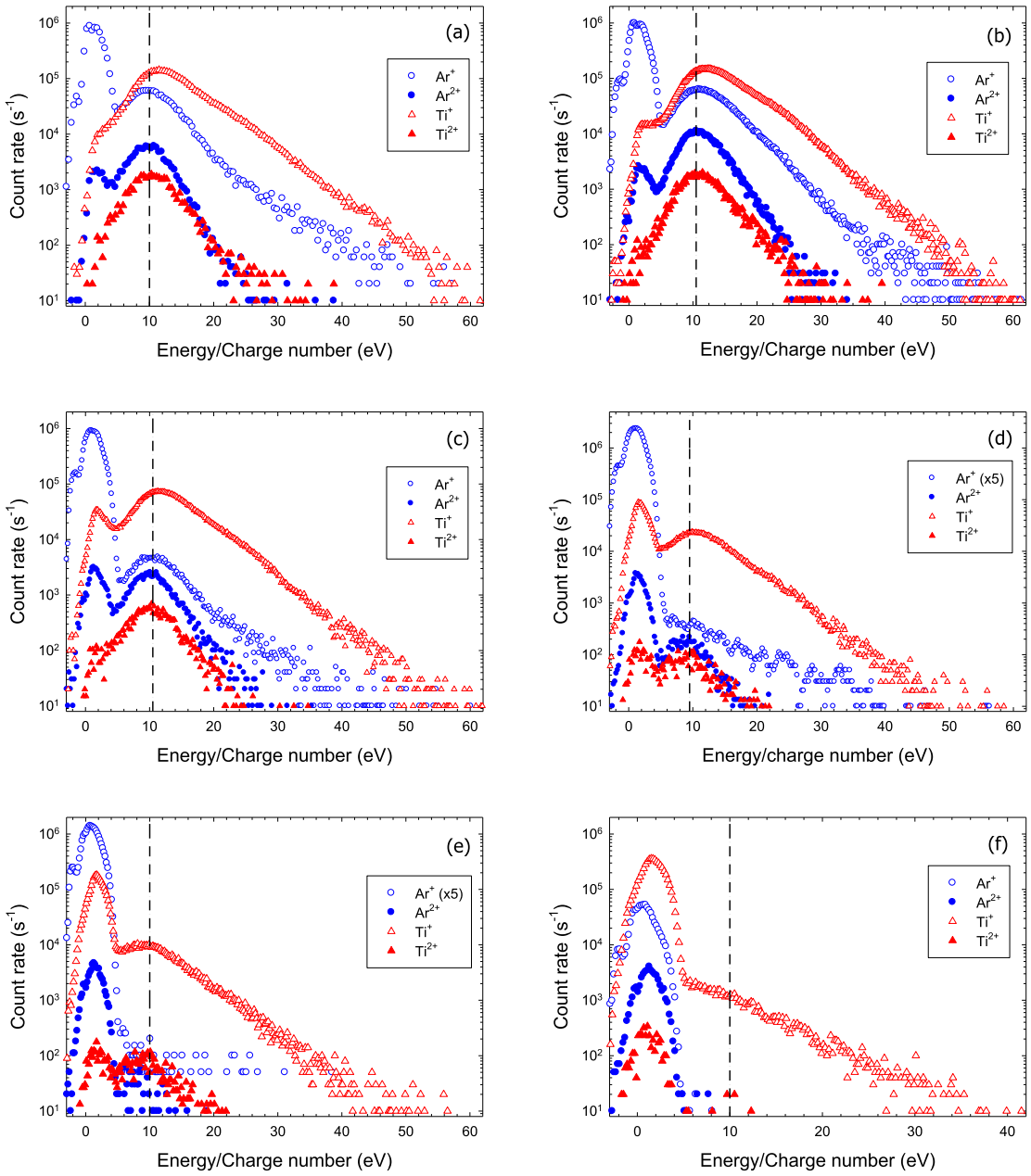

Figure 2. Energy distribution of Ar^+ (○, $m/z = 40$), Ar^{2+} (•, $m/z = 20$), Ti^+ (△, $m/z = 48$), and Ti^{2+} (▲, $m/z = 24$) ions *versus* kinetic energy E divided by the charge number q at argon gas pressures of (a) 0.3 Pa, (b) 0.5 Pa, (c) 1.0 Pa, (d) 2.0 Pa, (e) 3.0 Pa, and (f) 5.5 Pa. Dash-dotted lines to guide the eye only.

0.5 Pa, Ar_2^+ ions also show a weak high-energy component, which extends beyond 12 eV. Energy distributions of Ti_2^+ ions distinctly differ from those of the two other dimer ions (figure 3(c)). At the lowest pressures of 0.3–1 Pa, Ti_2^+ ions display a single broad peak with a maximum of about 12 eV and a high-energy tail which extends beyond 25 eV.

The pressure dependence of the energy-integrated Ar^+, Ar^{2+}, Ti^+, Ti^{2+}, Ar_2^+, $ArTi^+$, and Ti_2^+ intensities is shown in figure 4. Within the investigated pressure range $p = 0.3$–5.5 Pa the intensity of Ar^+ ions drops by more than one order of magnitude. The energy-integrated intensity of Ti^+ ions follows the decreasing Ar^+ intensity up to a pressure of 2 Pa and then increases again; this increase compensates most of the decreasing Ar^+ intensity. It eventually indicates the transition from an argon-burning to a titanium-burning plasma. The intensity of doubly charged Ar^{2+} and Ti^{2+} ions decreases with increasing pressure up to $p = 2$ Pa and then remains approximately constant. Figure 5 separately displays the pressure dependence of the low-energy and the high-energy component. The low-energy component of all investigated species increases with increasing pressure, except for Ar^+ ions. Ti^+ display the strongest increase by more than one order of magnitude over the investigated pressure range whereas the intensity increase of Ar^{2+} and Ti^{2+} is comparatively modest. Part of the decreasing

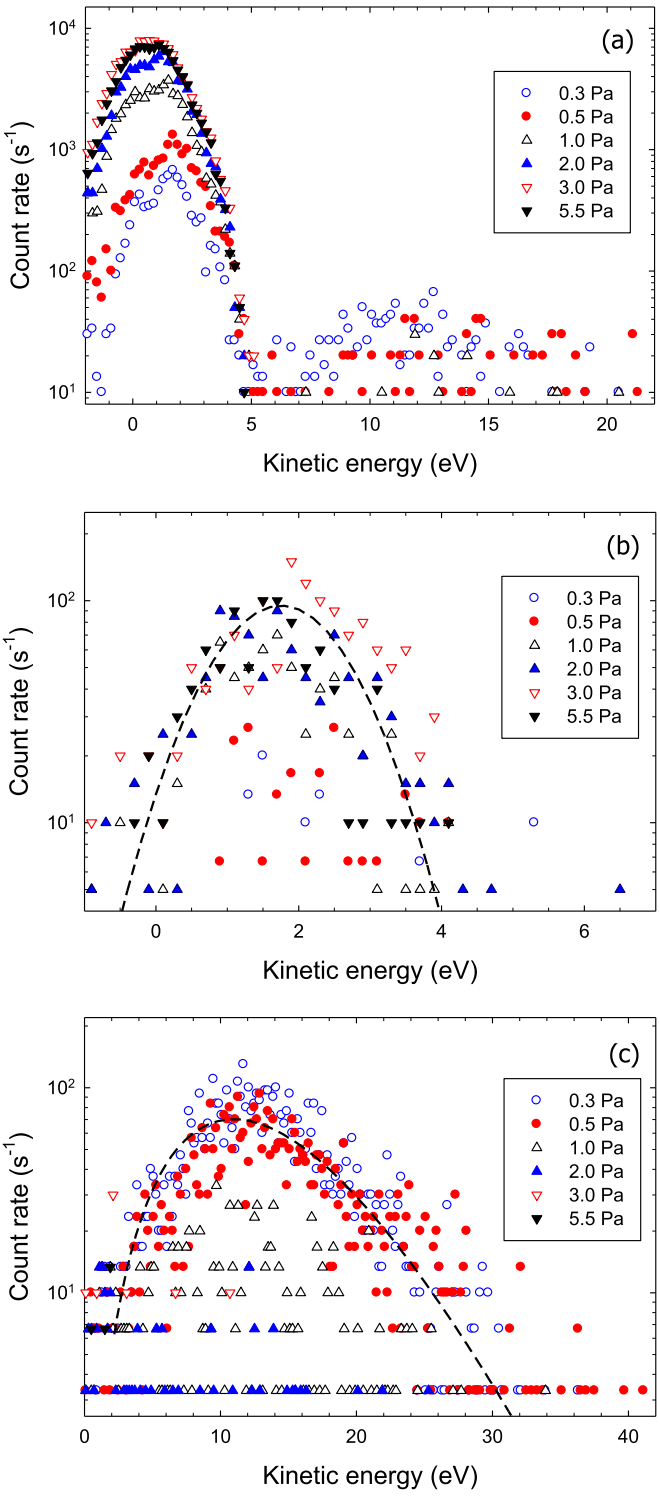

Figure 3. Energy distribution of (a) Ar_2^+ ($m/z = 80$), (b) $ArTi^+$ ($m/z = 88$), and (c) Ti_2^+ ($m/z = 96$) ions at argon pressures of 0.3 Pa (○), 0.5 Pa (•), 1.0 Pa (△), 2.0 Pa (▲), 3.0 Pa (▽), and 5.5 Pa (▼). Dashed lines to guide the eye only. Discharge power $P = 150$ W.

Ar^+ intensity is due to the high-energy component which decreases by several orders of magnitude over the same pressure range.

The strong decrease of the high-energy component of Ar^+ and Ar^{2+} ions can be explained by resonant charge changing collisions, e.g. $Ar^+ + Ar \rightarrow Ar + Ar^+$, through which a fast ion is neutralised and a slow ion is generated. The estimated mean free path of 10 eV Ar^+ and Ar^{2+} ions in Ar gas at a pressure of 1 Pa, calculated with the help of known cross sections, is ≈0.9 cm and 1.6 cm, respectively [26, 27]. Charge exchange of Ti^+ or Ti^{2+} ions with ground state Ar atoms is a non-resonant process. The corresponding cross sections are expected to be smaller and the mean free path of the energetic Ti^+ and Ti^{2+} ions is thus larger compared to the resonant case.

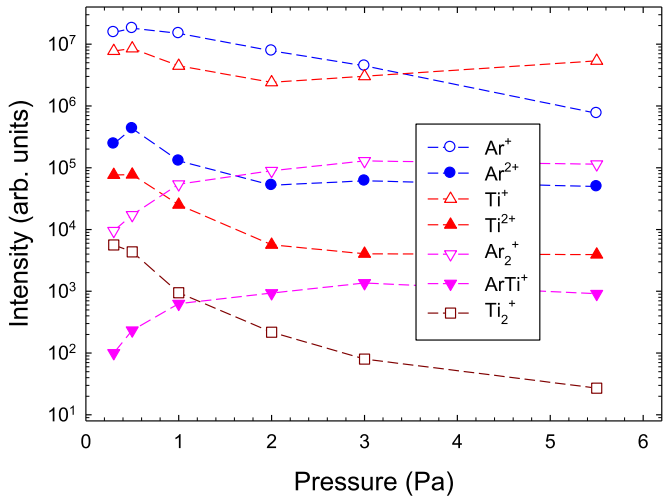

Figure 4. Pressure dependency of energy-integrated Ar^+ ($m/z = 40$, ∘), Ar^{2+} ($m/z = 20$, •), Ti^+ ($m/z = 48$, △), Ti^{2+} ($m/z = 24$, ▲), Ar_2^+ ($m/z = 80$, ▽), $ArTi^+$ ($m/z = 88$, ▼), and Ti_2^+ ($m/z = 96$, □) ion intensity. Ar gas, discharge power $P = 150$ W. Dashed lines to guide the eye only.

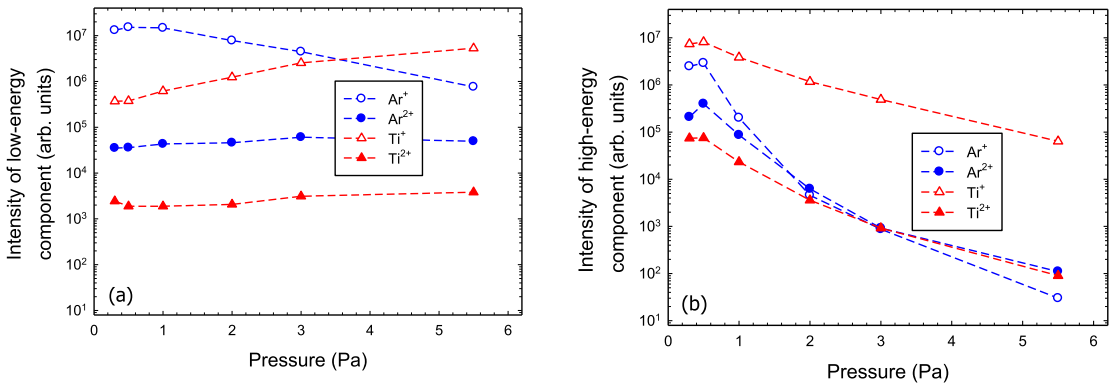

Figure 5. Pressure dependency of the (a) low-energy and (b) high-energy component of Ar^+ ($m/z = 40$, ∘), Ar^{2+} ($m/z = 20$, •), Ti^+ ($m/z = 48$, △), and Ti^{2+} ($m/z = 24$, ▲) ions. Ar gas, discharge power $P = 150$ W. Dashed lines to guide the eye only.

The energy-integrated intensities of Ar_2^+ and $ArTi^+$ ions show a pronounced increase with increasing gas pressure (figure 4). This observation can be explained by the formation process, in particular, the three-body collisions of Ar^+ or Ti^+ ions with two ground state Ar atoms and the associate ionisation of ground state Ar or Ti atoms with excited Ar^* atoms [20]. The decreasing intensity of Ti_2^+ ions is not fully understood yet. A possible explanation could be fragmentation in collisions with gas atoms as was observed for negatively charged cluster ions [28]

3.2. Ar+O_2 gas mixture

Measurements were also performed with an Ar + O_2 gas mixture. Compared to the pure Ar case, the mass spectrum of positive ions displays additional ion peaks at mass numbers $m/z = 16$, 32, and 64 which are attributed to O^+, O_2^+, and TiO^+ ions, respectively (figure 1). The mass spectrum of negative ions is largely composed of O^- and O_2^- ions.

3.2.1. Positive ions

Energy distributions of O^+, O_2^+, Ar^+, and Ar^{2+} ions are displayed in figure 6. Energy distributions of Ar^+ ions of the Ar+O_2 gas mixture are similar compared to the pure Ar case, i.e. they are composed of a pronounced low-energy component and a high-energy component which disappears at larger pressures. Noticeable differences are a smaller high-energy component and an apparent shift of the energy spectrum by approximately –2 eV to more negative energies. The shift can be explained by a reduced plasma potential due to the presence of negative ions. The energy distribution of molecular O_2^+ ions displays almost identical low-energy and high-energy components with a similar pressure dependence as for Ar^+ ions. At the lowest pressure of 0.38 Pa, the O_2^+ energy

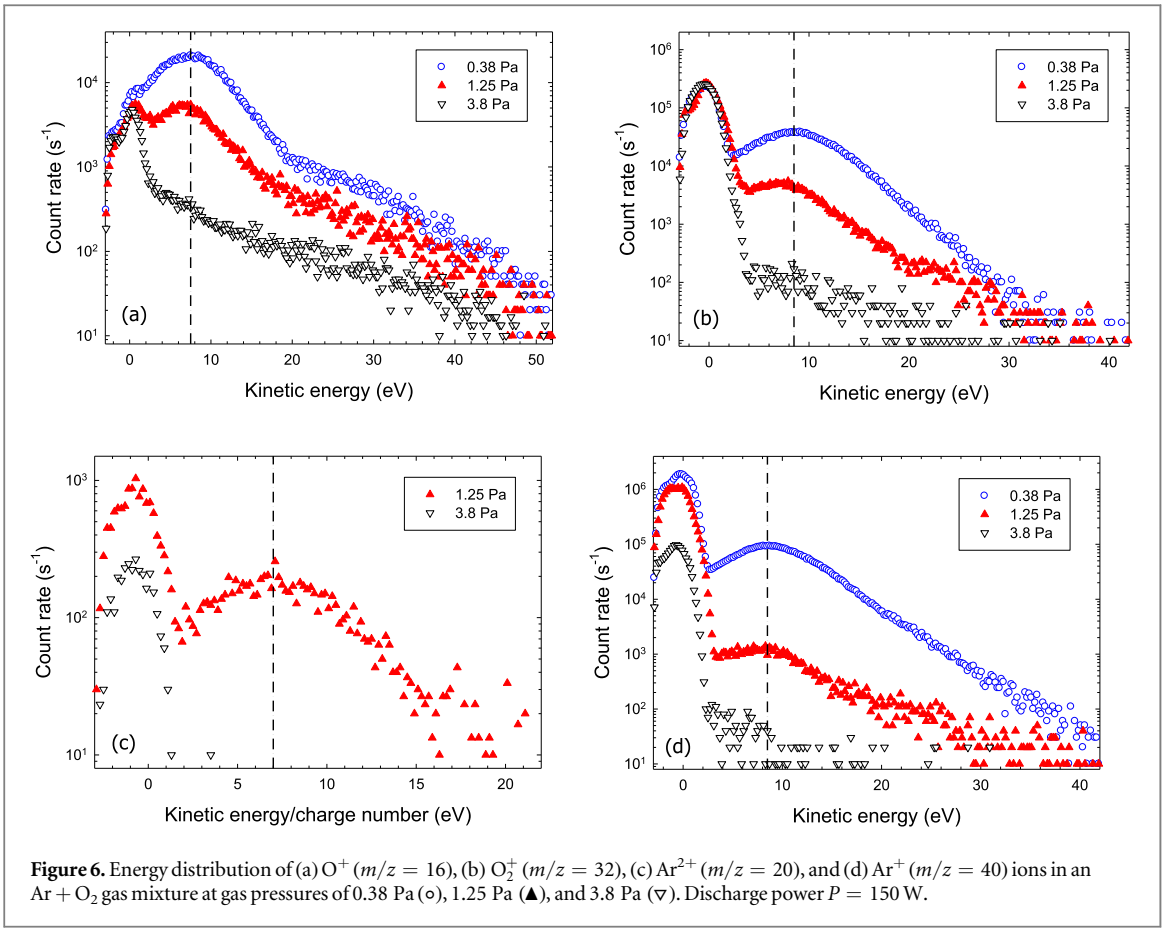

Figure 6. Energy distribution of (a) O^+ ($m/z = 16$), (b) O_2^+ ($m/z = 32$), (c) Ar^{2+} ($m/z = 20$), and (d) Ar^+ ($m/z = 40$) ions in an $Ar + O_2$ gas mixture at gas pressures of 0.38 Pa (○), 1.25 Pa (▲), and 3.8 Pa (▽). Discharge power $P = 150$ W.

distribution extends up to about 30 eV which is 10 eV less compared to Ar^+ ions. In addition to the other two components, energy distributions of O^+ ions display an extended high energy tail. The high-energy tail points to a sputtering contribution from absorbed oxygen atoms on the target. It is evident from figure 6(a) that the broad peak at ≈7.5 eV resembling the regular high-energy component vanishes with increasing pressure whereas the extended tail displays a much weaker pressure dependence. The broad peak can be explained by a positive plasma potential (hump) which in the $Ar+O_2$ gas mixture is about 2 V lower compared to the pure Ar case. The potential hump is located close to the target and thus far away from the entrance orifice of the detector. In order to explain the non-vanishing of the extended tail we have to consider that the majority of sputtered species is neutral and that ionisation takes place in some distance from the target, ie., closer to the entrance of the orifice.

Energy distributions of Ti^+ and TiO^+ ions are displayed in figure 7. Ti^+ and TiO^+ ions display rather similar energy distributions and intensities which are characterised by a broad peak with a maximum intensity at ≈10 eV. The broad peak vanishes with increasing pressure and a weak low-energy component remains.

Figure 8 displays the energy-integrated intensity of O^+, O_2^+, Ar^+, Ar^{2+}, Ti^+, and TiO^+ ions as a function of the $Ar+O_2$ gas pressure. The comparison shows that with the exception of O_2^+ all ion intensities decrease with increasing pressure. At small pressures the $Ar+O_2$ discharge is dominated by Ar^+ ions, whereas O_2^+ ions dominate at the largest pressure. Intensities of O^+ are about one order of magnitude smaller compared to O_2^+ ions. The intensity of oxidised TiO^+ is somewhat larger compared to Ti^+ ions; the TiO^+/Ti^+ ratio increases from 1.2 at $p = 0.38$ Pa to 4.5 at $p = 3.8$ Pa. Overall, the Ti^+ ion intensity of the $Ar+O_2$ gas mixture is about 2 orders of magnitude smaller compared to the pure Ar case. Comparable observations were made for sputtering of neutral atoms in a magnetron discharge [29]. It can be partly explained by a smaller sputtering rate from an oxidised target [17, 18].

3.2.2. Negative ions

Energy distributions of negatively charged O^- and O_2^- ions are shown in figure 9. O^- ions display a low-energy component and a high-energy component which peak at different energies compared to positive ions, i.e. at 1.5–5.5 eV and 25–35 eV. It appears likely that O^- ions are formed in gas phase collisions via dissociative attachment, e.g. $e^- + O_2 \rightarrow O^- + O$ [30]. The high-energy component above 20 eV is believed to arise from O sputtering off the oxygen-covered surface and subsequent negative ion formation in the plasma. It contributes about 35% and thus is a non-negligible portion to the energy-integrated O^- intensity. Formation of O_2^- ions can proceed in gas phase collisions via three-body electron attachment, e.g. $e^- + O_2 + M \rightarrow O_2^- + M$, where M is a

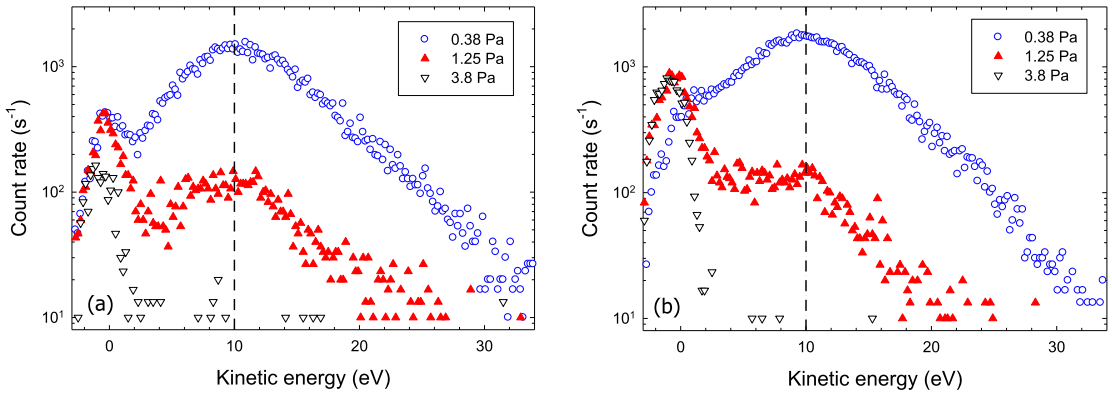

Figure 7. Energy distribution of (a) Ti^+ ($m/z = 48$) and (b) TiO^+ ($m/z = 64$) ions in an $Ar + O_2$ gas mixture at gas pressures of 0.38 Pa (○), 1.25 Pa (▲), and 3.8 Pa (▽). Discharge power $P = 150$ W.

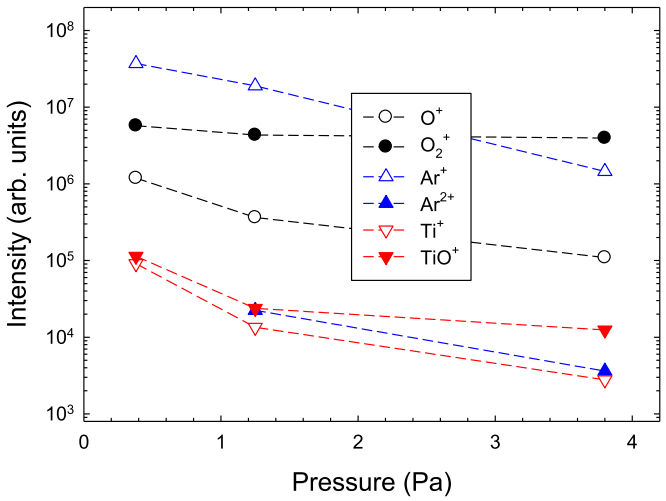

Figure 8. Pressure dependency of energy-integrated O^+ ($m/z = 16$, ○), O_2^+ ($m/z = 32$, •), Ar^+ ($m/z = 40$, △), Ar^{2+} ($m/z = 20$, ▲), Ti^+ ($m/z = 48$, ▽), and TiO^+ ($m/z = 64$, ▼) ion intensity. Ar+O2 gas mixture. Discharge power $P = 150$ W. Dashed lines to guide the eye only.

participating particle (electron, atom, ion, ...), in collisions with O^- ions, e.g. $O^- + O_2 \rightarrow O + O_2^-$ [31], or through charge transfer reactions with energetic atoms or ions, e.g. $A + O_2 \rightarrow A^+ + O_2^-$ [32]. Energy-integrated intensities of O_2^- are more than 30× smaller compared to O^-, which can be explained by the smaller formation rates in qualitative agreement with theoretical results [31]. The energy distribution of O_2^- is characterized by a dominant low-energy component while an eventual high-energy component is absent. The low-energy component seem to split into two parts with a lower maximum at ≈0 eV and a second maximum at ≈4.5 eV. No explanation for this behaviour has been found yet.

4. Conclusions

Formation of singly and doubly charged Ar^{q+} and Ti^{q+} ($q = 1, 2$) monomer and of Ar_2^+, $ArTi^+$, and and Ti_2^+ dimer ions in a direct current magnetron discharge with a Ti target and with pure argon as working gas was investigated by means of energy-dispersive mass spectrometry. In general, the measured energy distributions consist of low- and high-energy components. The low-energy component is due to gas phase collisions. The high-energy component results from a field reversal by a potential hump in some distance from the cathode. As a consequence, the kinetic energy of doubly charged ions is twice as large compared to singly charged ions. Formation of Ar_2^+ and $ArTi^+$ dimer ions shows a pronounced pressure dependence that is attributed to the formation processes inside the plasma region. Ti_2^+ ions are formed by direct sputtering of Ti_2 molecules and the subsequent ionization in the plasma. The pronounced decrease of Ti_2^+ intensity with gas pressure is not fully understood yet.

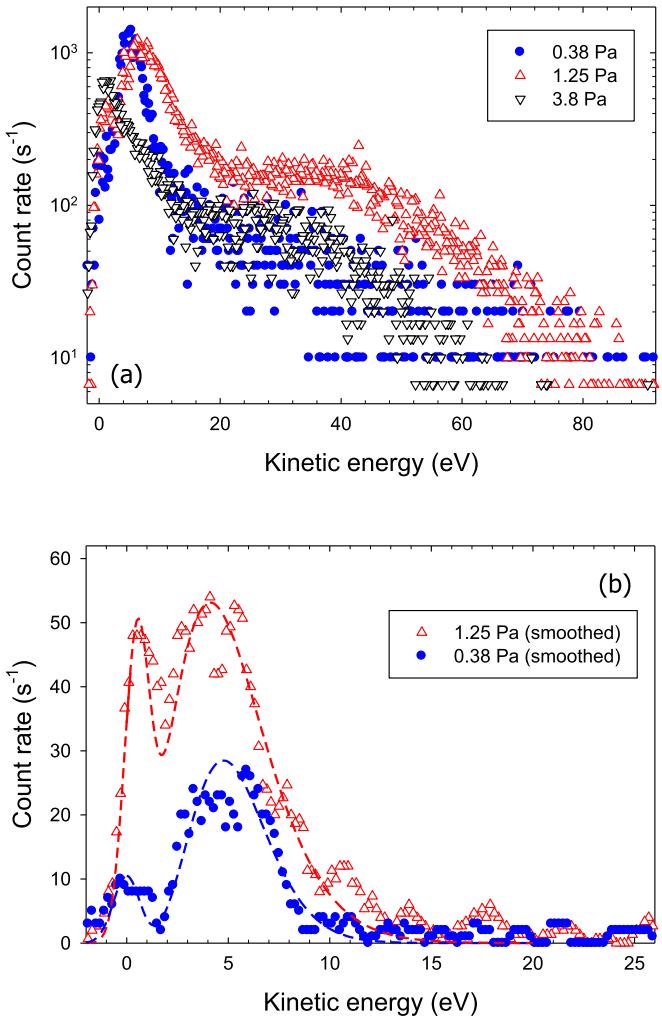

Figure 9. Energy distribution of negatively charged O^- ($m/z = 16$) and O_2^- ($m/z = 32$) ions in an Ar + O_2 gas mixture at gas pressures of 0.38 Pa, 1.25 Pa, and 3.8 Pa. Dashed lines to guide the eye only. Discharge power $P = 150$ W.

Addition of oxygen to the discharge leads to the formation of positively (O^+, O_2^+) and negatively charged (O^-, O_2^-) oxygen ions. Ar^+ and O_2^+ ions are the dominant positively charged ion species at low and high gas pressure, respectively. Intensities of other positive ion species are considerably smaller. In particular, the intensity of sputtered Ti^+ ions is significantly reduced in the Ar+O_2 gas mixture compared to the pure Ar case. TiO^+ ions with a slightly larger intensity compared to Ti^+ are additionally observed. However, this does not compensate for the strong reduction of the Ti^+ intensity which in part is caused by a lower sputtering yield. The negative ion mass spectrum is dominated by O^- ions. O_2^- ions are difficult to produce and the intensity is more than one of magnitude smaller compared to O^- ions. The present results shed new light on kinetic energy distribution of atomic and molecular plasma species and its control by a variation of gas density.

Acknowledgments

The work was partly supported by project no. 19-00579S of the Czech Science Foundation and by project no. SOLID21-CZ.02.1.01/0.0/0.0/16_019/0000760 of the Operational Programme Research, Development and Education financed by European Structural and Investment Funds and the Czech Ministry of Education, Youth and Sports.

ORCID iDs

R Hippler https://orcid.org/0000-0002-5956-3321
M Cada https://orcid.org/0000-0001-6826-983X

References

[1] Hippler R *et al* (ed) 2008 *Low Temperature Plasmas* vols 1 and 2 (Berlin: Wiley-VCH)
[2] Affinito J and Parsons R R 1984 *J. Vacuum Sci. Technol.* A **2** 1275
[3] Mientus R and Ellmer K 1999 *Surf. Coat. Technol.* **116–119** 1093
[4] Berg S and Nyberg T 2005 *Thin Solid Films* **476** 215
[5] Depla D, Heirwegh S, Mahieu S, Haemers J and Gryse R De 2007 *J. Appl. Phys.* **101** 013301
[6] Schiller S, Heisig U, Steinfelder K and Strumpfel J 1982 *Thin Solid Films* **96** 235
[7] Sproul W D and Tomashek J R *US Patent* 4428811(January 31, 1984)
[8] Sproul W D, Christie D J and Carter D C 2005 *Thin Solid Films* **491** 1
[9] Waits R K 1978 *J. Vac Sci. Technol.* **15** 171
[10] Thornton J A 1978 *J. Vac Sci. Technol.* **15** 179
[11] Misina M, Shaginyan L R, Macek K and Panjan P 2001 *Surf. Coat. Technol.* **142** 348
[12] Bradley J W, Bäcker H, Aranda-Gonzalvo Y, Kelly P J and Arnell R D 2002 *Plasma Sources Sci. Technol.* **11** 165
[13] Hippler R, Wrehde S, Stranak V, Zhigalov O, Steffen H, Tichy M, Quaas M and Wulff H 2005 *Contrib. Plasma Phys.* **45** 348
[14] Bohlmark J, Alami J, Christou C, Ehiasarian A P and Helmersson U 2005 *J. Vacuum Sci. Technol. A: Vacuum, Surfaces, and Films* **23** 18
[15] Hippler R, Steffen H, Quaas M, Röwf T, Tun T M and Wulff H 2004 *Advances in Solid State Physics* vol 44 ed B Kramer (Heidelberg: Springer) p 299
[16] Stranak V *et al* 2009 *J. Phys. D: Appl. Phys.* **42** 105204
[17] Gudmundsson J T, Lundin D, Brenning N, Raadu M A, Huo C and Minea T M 2016 *Plasma Sources Sci. Technol.* **25** 065004
[18] Hecimovic A, Corbella C, Maszl C, Breilmann W and von Keudell A 2017 *J. Appl. Phys.* **121** 171915
[19] Stranak V, Hubicka Z, Cada M, Bogdanowicz R, Wulff H, Helm C A and Hippler R 2018 *J. Phys. D: Appl. Phys.* **51** 095205
[20] Hippler R, Cada M, Stranak V, Hubicka Z and Helm C A 2017 *J. Phys. D: Appl. Phys.* **50** 445205
[21] Cada M, Hubicka Z, Adamek P, Kluson J and Jastrabik L 2011 *Surf. Coat. Technol.* **205** S317
[22] Sushkov V, Do H T, Cada M, Hubicka Z and Hippler R 2013 *Plasma Sources Sci. Technol.* **22** 015002
[23] Rosman K J R and Taylor P D P 1998 *Pure Appl. Chem.* **70** 217
[24] Anders A 2011 *Surf. Coat. Technol.* **205** S1
[25] Breilmann W, Maszl C, Benedikt J and von Keudell A 2013 *J. Phys. D: Appl. Phys.* **46** 485204
[26] Pullins S H, Dressler R A, Torrents R and Gerlich D 2000 *Z. Phys. Chem.* **214** 1279
[27] Okuno K 1986 *J. Phys. Soc. Jpn.* **55** 1504
[28] Welzel T, Naumov S and Ellmer K 2011 *J. Appl. Phys.* **109** 073302
[29] Wolter M, Do H T, Steffen H and Hippler R 2005 *J. Phys. D: Appl. Phys.* **38** 2390
[30] Gudmundsson J T and Thorsteinsson E G 2007 *Plasma Sources Sci. Technol.* **16** 399
[31] Gudmundsson J T, Kouznetsov I G, Patel K K and Lieberman M A 2001 *J. Phys. D: Appl. Phys.* **34** 1100
[32] Angelin E J and Hippler R 2013 *Phys. Rev.* A **87** 052704